HEALTH AND MEDICINE

A modular approach toward producing nanotherapeutics targeting the innate immune system

Mandy M. T. van Leent[1,2], Anu E. Meerwaldt[1,3], Alexandre Berchouchi[1], Yohana C. Toner[1], Marianne E. Burnett[1], Emma D. Klein[1], Anna Vera D. Verschuur[1], Sheqouia A. Nauta[1], Jazz Munitz[1], Geoffrey Prévot[1], Esther M. van Leeuwen[1], Farideh Ordikhani[4], Vera P. Mourits[5], Claudia Calcagno[1], Philip M. Robson[1], George Soultanidis[1], Thomas Reiner[6,7,8], Rick R. M. Joosten[9], Heiner Friedrich[9,10], Joren C. Madsen[11], Ewelina Kluza[10,12], Roy van der Meel[10,12], Leo A. B. Joosten[5], Mihai G. Netea[5,13], Jordi Ochando[4], Zahi A. Fayad[1], Carlos Pérez-Medina[14], Willem J. M. Mulder[1,10,12]*, Abraham J. P. Teunissen[1]*

Immunotherapies controlling the adaptive immune system are firmly established, but regulating the innate immune system remains much less explored. The intrinsic interactions between nanoparticles and phagocytic myeloid cells make these materials especially suited for engaging the innate immune system. However, developing nanotherapeutics is an elaborate process. Here, we demonstrate a modular approach that facilitates efficiently incorporating a broad variety of drugs in a nanobiologic platform. Using a microfluidic formulation strategy, we produced apolipoprotein A1–based nanobiologics with favorable innate immune system–engaging properties as evaluated by in vivo screening. Subsequently, rapamycin and three small-molecule inhibitors were derivatized with lipophilic promoieties, ensuring their seamless incorporation and efficient retention in nanobiologics. A short regimen of intravenously administered rapamycin-loaded nanobiologics (mTORi-NBs) significantly prolonged allograft survival in a heart transplantation mouse model. Last, we studied mTORi-NB biodistribution in nonhuman primates by PET/MR imaging and evaluated its safety, paving the way for clinical translation.

INTRODUCTION

In the past decade, immunotherapy has emerged as a revolutionary cancer treatment. Clinically relevant immunotherapies, such as chimeric antigen receptor T cells and immune checkpoint inhibition, engage the adaptive immune system and mount a highly specific response (*1*). While the value of these therapeutic approaches is indisputable, targeting the innate immune system also holds great promise (*1*, *2*) but remains largely unexplored.

The innate immune system provides nonspecific protection against invading pathogens through myeloid cells with diverse functions. In addition, myeloid cells, in particular, dendritic cells and macrophages, can invoke an antigen-specific adaptive immune response. Myeloid cells are activated by pathogen- or damage-associated molecular patterns through pattern recognizing receptors. Upon their activation, myeloid cells undergo metabolic and epigenetic rewiring, leading to a hypersensitivity toward subsequent encounters with both related and unrelated pathogens. This phenomenon is termed "trained immunity" and can persist for several months (*3*).

Therapeutically managing trained immunity is a promising treatment paradigm for diseases characterized by excessive inflammation, such as autoimmune disorders, cardiovascular disease, and allograft rejection (*1*, *2*). This can be achieved by treating myeloid cells and their progenitors with drugs that modulate the metabolic or epigenetic programming underlying trained immunity. However, exploiting small-molecule inhibitors in this manner is hampered by the low myeloid cell specificity of these drugs.

Here, we report on a nanobiologic platform composed of apolipoprotein A1 (apoA-I)–based nanomaterials that efficiently target myeloid cells and their bone marrow progenitors. To enable nanobiologics' modular functionalization with small-molecule inhibitors, we established a strategy in which these drugs are derivatized with biocleavable lipophilic promoieties (*4*). Using microfluidic formulation technology, we generated differently sized nanobiologics ranging from 20 to 120 nm. Their biodistribution and immune cell specificity were assessed by combining in vivo positron emission tomography (PET) imaging and ex vivo gamma counting with flow cytometry assays. On the basis of this screening, the 35-nm-sized nanobiologic formulation was selected for further studies. To investigate the approach's versatility, we loaded the 35-nm-sized nanobiologics with different small-molecule inhibitors, including the mammalian target of rapamycin (mTOR) inhibitor rapamycin, and found that our prodrug approach resulted in universal and highly efficient drug incorporation and retention. The immunotherapeutic benefits of these drug-loaded nanobiologics were subsequently

[1]Biomedical Engineering and Imaging Institute, Icahn School of Medicine at Mount Sinai, New York, NY, USA. [2]Department of Medical Biochemistry, Amsterdam University Medical Centers, Amsterdam, Netherlands. [3]Biomedical MR Imaging and Spectroscopy Group, Center for Image Sciences, University Medical Center Utrecht/Utrecht University, Utrecht, Netherlands. [4]Department of Oncological Sciences, Icahn School of Medicine at Mount Sinai, New York, NY, USA. [5]Department of Internal Medicine, Radboud Center for Infectious Diseases (RCI), Radboud Institute of Molecular Life Sciences (RIMLS), Radboud University Medical Center, Nijmegen, Netherlands. [6]Department of Radiology, Memorial Sloan Kettering Cancer Center, New York, NY, USA. [7]Department of Radiology, Weill Cornell Medical College, New York, NY, USA. [8]Chemical Biology Program, Memorial Sloan Kettering Cancer Center, New York, NY, USA. [9]Center of Multiscale Electron Microscopy, Department of Chemical Engineering and Chemistry, Eindhoven University of Technology, PO Box 513, 5600 MB Eindhoven, Netherlands. [10]Institute for Complex Molecular Systems, Eindhoven University of Technology, Eindhoven, Netherlands. [11]Center for Transplantation Sciences and Division of Cardiac Surgery, Department of Surgery, Massachusetts General Hospital, Boston, MA, USA. [12]Laboratory of Chemical Biology, Department of Biochemical Engineering, Eindhoven University of Technology, Eindhoven, Netherlands. [13]Department for Genomics & Immunoregulation, Life and Medical Sciences Institute (LIMES), University of Bonn, Bonn, Germany. [14]Centro Nacional de Investigaciones Cardiovasculares (CNIC), Madrid, Spain.
*Corresponding author. Email: bram.teunissen@mssm.edu (A.J.P.T.); willem.mulder@mssm.edu (W.J.M.M.)

assessed physicochemically and in vitro. On the basis of these findings, we subjected the mTOR inhibiting nanobiologics (mTORi-NBs) to an optimization and in vivo evaluation process. In addition to experiments in a heart allograft transplantation mouse model, we studied mTORi-NBs' biodistribution and toxicity profile in non-human primates.

RESULTS

Developing nanobiologics with high affinity for myeloid cells

Efficient nanotherapeutic modulation of the innate immune system requires a biocompatible nanocarrier with high affinity for innate immune cell–rich organs (i.e., the spleen and bone marrow). High-density lipoprotein (HDL) is a natural nanocarrier responsible for the transport of fat and other biomolecules (*5*). apoA-I is the major protein constituent of native HDL and interacts with scavenger receptors and the adenosine triphosphate (ATP)–binding cassette transporters ABCA1 and ABCG1, abundantly present on myeloid cells (*6*). On the basis of apoA-I, we developed innate immune cell–targeting nanocarriers, which we termed nanobiologics. We here present four differently sized nanobiologics composed of phospholipid 1-palmitoyl-2-oleoyl-glycero-3-phosphocholine (POPC), lysolipid 1-palmitoyl-2-hydroxy-sn-glycero-3-phosphocholine (PHPC), apoA-I, and cholesterol (Fig. 1A) (*7*–*9*). The triglyceride tricaprylin—chosen because of its high biocompatibility (*10*, *11*)—was incorporated in the three largest nanobiologics. The nanobiologics were produced by mixing a phosphate-buffered saline (PBS) solution of apoA-I with an acetonitrile solution containing POPC and PHPC lipids, cholesterol, and optional tricaprylin using a microfluidic chip setup. By controlling flow rates and the acetonitrile solution composition, nanobiologics with sizes of 20, 35, 65, and 120 nm were obtained (dispersities typically below 0.2; fig. S1A). Using this easily scalable approach, a single person was able to formulate up to 12 batches of nanobiologics per day.

Next, we studied the physicochemical properties of the nanobiologics. We determined their stability when stored in PBS at 4°C. Dynamic light scattering (DLS) measurements showed that the 20-, 35-, and 65-nm formulations remained stable for at least 10 days, while the 120-nm formulation gradually reduced in size (Fig. 1B), which was accompanied by the appearance of a triglyceride phase on top of the nanobiologic emulsion. Therefore, we subsequently focused on the development and evaluation of the 20-, 35-, and 65-nm-sized formulations. Cryogenic transmission electron microscopy (cryo-TEM) analyses uncovered the 20-nm nanobiologic as circular shapes, which match the discoidal morphology we previously observed by TEM and cryo-TEM for similar formulations (*7*, *12*). In contrast, the 35- and 65-nm nanobiologics have uniform contrast and a seemingly spherical shape as a result of their tricaprylin core (Fig. 1C).

To determine pharmacokinetics and biodistribution in mice, nanobiologics were radiolabeled by functionalizing apoA-I with the chelator deferoxamine (DFO). The DFO-decorated nanobiologics were subsequently used to chelate the radioisotope ^{89}Zr using a procedure we previously developed (*13*). The resulting ^{89}Zr-radiolabeled nanobiologics were intravenously administered to C57BL/6 mice (n = 7 for each formulation). At 24 hours after administration, in vivo PET/computed tomography (CT) imaging was performed (n = 2 per nanobiologic; Fig. 1D), while nanobiologic blood half-life and uptake in major organs was determined by ex vivo gamma counting (n = 5 per nanobiologic; Fig. 1, E and F, fig. S1B, and table S1). We found a similar in vivo behavior for all three formulations, with the 20-nm nanobiologics circulating slightly longer than the 35- and 65-nm nanobiologics (Fig. 1E and table S2). As expected, we found high nanobiologic uptake in the spleen and clearance organs such as the liver and kidneys (*14*). Relative to the liver, we measured a significantly higher nanobiologic uptake in the bone marrow for the 35-nm formulation compared to the 65-nm variant. Although not statistically significant, a similar trend was observed for the spleen-to-liver and lymph node–to–liver ratios (Fig. 1F and fig. S1C). To analyze nanobiologic behavior on a cellular level, the highly lipophilic dye $DiOC_{18}$ (3) was incorporated and intravenously administered to C57BL/6 mice. Animals were sacrificed 24 hours later, and cellular uptake of $DiOC_{18}$ (3) was assessed by flow cytometric analyses of leukocytes in the bone marrow, blood, and spleen. All nanobiologics displayed a high affinity for myeloid cells as well as uptake in hematopoietic stem and progenitor cells (HSPCs), with negligible uptake by B and T lymphocytes (Fig. 1G and fig. S2, A and B). On the basis of its high bone marrow and Ly6C^{hi} monocyte uptake, we selected the 35-nm nanobiologic for ensuing studies.

Fluorescent model drug delivery to myeloid cells

The efficient exploitation of the 35-nm-sized nanobiologic as an immunotherapeutic requires high compatibility between its triglyceride core and therapeutic payload. As physicochemical properties widely vary, we set out to develop a prodrug approach that enhances the therapeutic payload's lipophilicity by functionalizing it with apolar promoieties. We first evaluated this approach's potential using BODIPY carboxylic acid (BODIPY) as a model drug, allowing the in vivo evaluation of the 35-nm-sized nanobiologic by flow cytometric analyses. Lipophilic BODIPY derivatives were created by esterifying this compound with either an aliphatic C_{18} chain (BODIPY-aliphatic) or cholesterol (BODIPY-cholesterol; Fig. 2A and fig. S3). The aliphatic promoieties were chosen because these chains are the predominant constituents of both the nanobiologic triglyceride core and its phospholipid corona. As cholesterol stably incorporates in native lipoproteins, we also used this promoiety to facilitate payload incorporation into nanobiologics (*15*). Both hydrolysable model prodrugs were successfully incorporated in the 35-nm nanobiologics with recoveries of approximately 60%, while the recovery of unfunctionalized BODIPY was negligible (defined as 100% * the amount of drug in the nanobiologics/the starting amount; Fig. 2, B and C, see table S3 for analytical methods). Dialyzing the nanobiologics against fetal bovine serum (FBS) at 37°C [10-kDa MWCO (molecular weight cut-off)] for 24 hours did not result in notable prodrug release or hydrolysis (Fig. 2D). Although these conditions do not fully mimic the in vivo environment, these results corroborate the nanotherapeutics' stability. We next set out to examine nanobiologic delivery of BODIPY model prodrugs to HSPCs and myeloid cells in the bone marrow. Formulations containing 1×, 5×, or 25× a reference amount of either BODIPY-aliphatic or BODIPY-cholesterol (Fig. 2E) were intravenously administered to mice at a fixed nanobiologic dose, resulting in varying doses of BODIPY model prodrug (0.1, 0.5, and 2.5 mg/kg). For nanobiologics loaded with BODIPY-aliphatic, flow cytometry analysis revealed a nearly linear relationship between the nanobiologic payload and the mean BODIPY fluorescence intensity in bone marrow Ly6C^{hi} monocytes. BODIPY-cholesterol–loaded nanobiologics displayed a similar but slightly different behavior, while

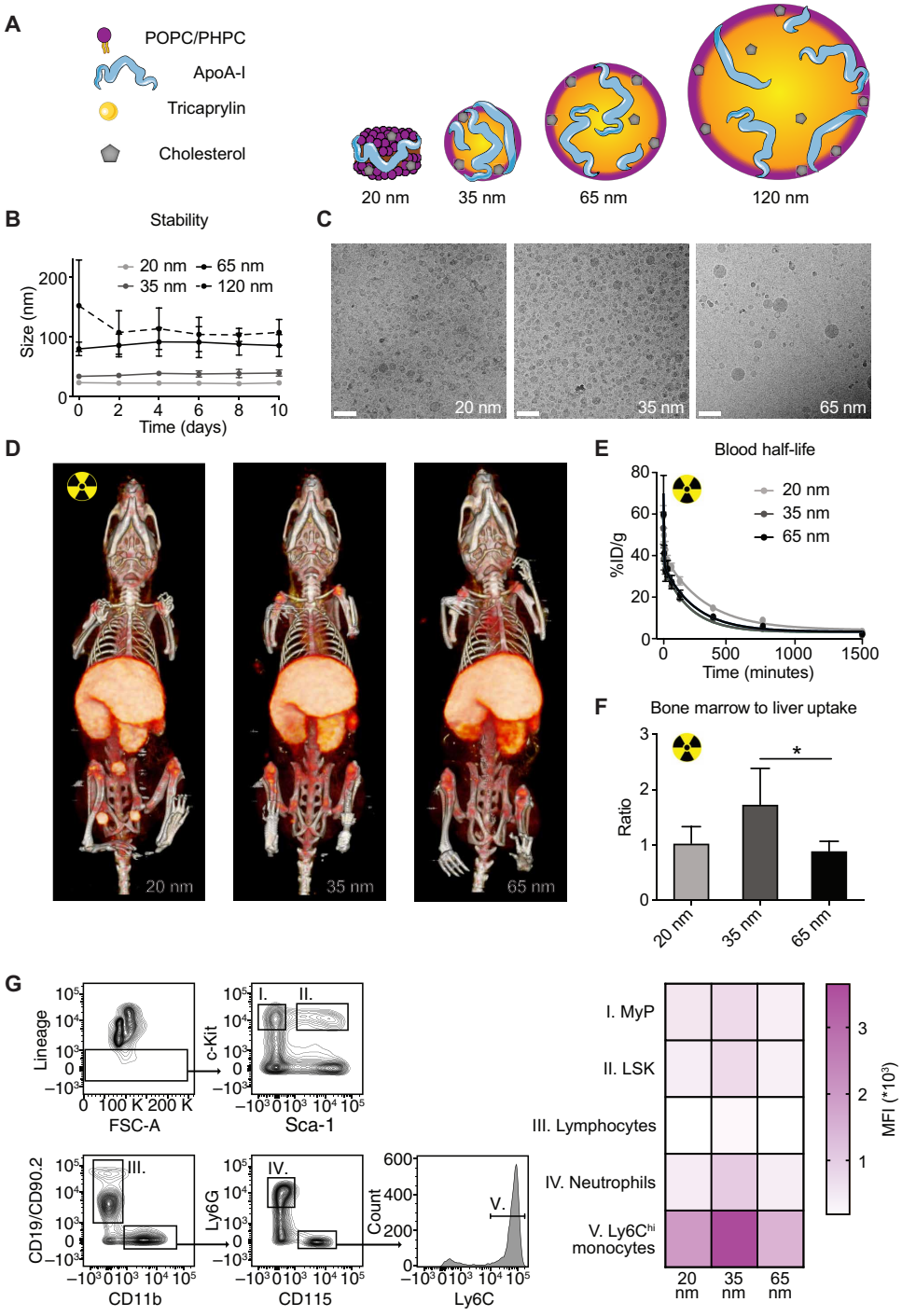

Fig. 1. Investigating the nanobiologics' stability, biodistribution, and immune cell engagement. (**A**) Composition and morphology of the nanobiologics, formulated by microfluidic mixing. (**B**) Size and stability of the nanobiologics in PBS at 4°C, as measured by DLS. The mean of the number average size distribution is reported. While the 20-, 35-, and 65-nm formulations remained stable, the 120-nm variant shrunk over time and was therefore excluded from subsequent experiments; $n = 3$ for each nanobiologic size. (**C**) Representative cryo-TEM images of the 20-, 35-, and 65-nm-sized nanobiologics. Scale bar, 100 nm. (**D** to **F**) C57BL/6 mice were intravenously injected with ^{89}Zr-labeled nanobiologics. (D) Representative maximum intensity projections of PET/CT scans performed 24 hours after injection. (E) Nanobiologics' blood pharmacokinetics were fitted with a biexponential decay function; $n = 5$ per formulation. (F) Nanobiologic uptake in the femur's bone marrow divided by nanobiologic uptake in the liver, measured at 24 hours after injection. (**G**) C57BL/6 mice were injected with $DiOC_{18}(3)$-labeled nanobiologics, and $DiOC_{18}(3)$ uptake was measured 24 hours after injection in various bone marrow cell populations by flow cytometry. Gating strategy and average mean fluorescence intensity (MFI) values are shown; $n = 4$ per formulation. MyP, myeloid progenitors; LSK, Lin$^-$ Sca-1$^+$ and c-Kit$^+$. Data in (B), (E), and (F) are presented as means ± SD. *$P < 0.05$.

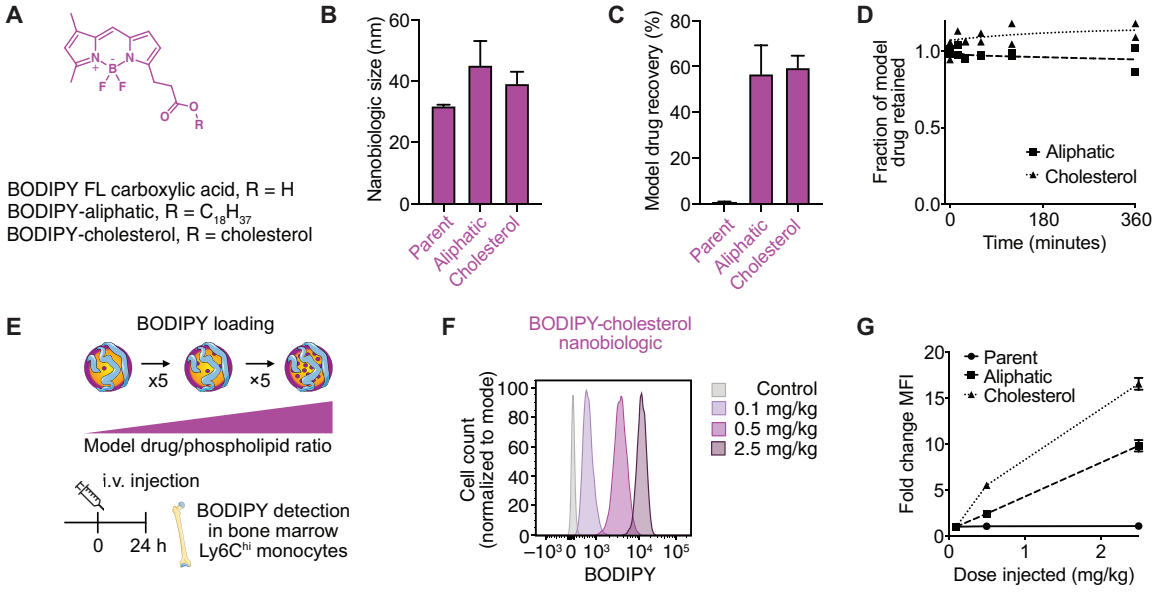

Fig. 2. Assessing the nanobiologics' ability to deliver drugs to the bone marrow. (**A**) Molecular structure of the fluorescent model drug BODIPY FL carboxylic acid as well as aliphatic and cholesterol functionalized derivatives. (**B**) Size of nanobiologics loaded with BODIPY or its derivatives as measured by DLS. The mean of the number average size distribution is displayed; $n = 3$. (**C**) Recovery of BODIPY and its derivatives as measured by high-performance liquid chromatography (HPLC), defined as the amount of (pro)drug in the nanobiologics divided by the amount used for their formulation; $n = 2$. (**D**) Release rate of the BODIPY derivatives from the nanobiologics when dialyzed against FBS at 37°C (10-kDa MWCO), as measured by HPLC. Data points are fitted with a biexponential decay function; $n = 2$. (**E** to **G**) Nanobiologics were formulated containing increasing amounts of either BODIPY-aliphatic or BODIPY-cholesterol. C57BL/6 mice were injected with identical doses of nanobiologics, leading to the administration of varying amounts of BODIPY model prodrugs; e.g., nanobiologics loaded with 5× more fluorophore were injected at a 5× higher fluorophore dose. Twenty-four hours after injection, MFI of Ly6C^{hi} monocytes was measured by flow cytometry. (E) Schematic overview of the experimental design. (F) Representative histograms of BODIPY signal in bone marrow Ly6C^{hi} monocytes from mice injected with increasing doses of BODIPY-cholesterol, but the same amount of nanobiologic. (G) MFI of the bone marrow's Ly6C^{hi} monocytes after administering nanobiologics loaded with various amounts of BODIPY-aliphatic or BODIPY-cholesterol; $n = 4$. Lines are to guide the eye. Data in (B) to (D) and (G) are represented as means ± SD. i.v., intravenous.

no increase in fluorescence signal was observed after administering identical doses of bare BODIPY (Fig. 2, F and G). The differences in mean fluorescence intensity (MFI) between the two types of model prodrugs likely stem from differences in their distribution within the nanocarrier (*4*, *16*). These results show that our combined nanobiologic and lipophilic prodrug approach can be used to efficiently deliver drugs to myeloid (progenitor) cells in the bone marrow.

Establishing and screening nanobiologics loaded with different drugs

After developing an effective drug loading strategy for nanobiologics, we set out to investigate the approach's versatility. For this purpose, we selected four (small molecule) drugs based on their ability to inhibit trained immunity by targeting specific metabolic or epigenetic processes. These drugs vary greatly in function, size, and physicochemical properties (Fig. 3A). Diethyl malonate is a low–molecular weight and highly water-soluble prodrug for malonic acid, which reduces mitochondrial reactive oxygen species production by inhibiting succinate oxidation and thereby reduces inflammation (*17*). (+)-JQ1 is a moderately sized and relatively rigid drug that targets bromodomains (*18*). It suppresses inflammation, atherogenesis, and various forms of cancers in mice, but it is currently not used in humans because of its short biological half-life. GSK-J4 is a moderately sized and more flexible compound that inhibits H3K27me$_3$ demethylases, thereby reducing macrophages' proinflammatory response to lipopolysaccharide (LPS) stimulation (*19*). Although this drug's active form consists of the carboxylic acid form (GSK-J1), the ethyl ester prodrug (GSK-J4) is used to achieve efficient cell penetration (*19*). Last, rapamycin is a relatively large drug that inhibits the mTOR pathway, which plays a central role in trained immunity regulation (*20*).

Using the same lipophilic prodrug strategy as used for the BODIPY model prodrugs, we functionalized malonate, rapamycin, (+)-JQ1, and GSK with either cholesterol or a C$_{18}$ aliphatic chain (fig. S4). While malonate, (+)-JQ1, and GSK analogs were synthesized using straightforward esterification chemistry, the derivatization of rapamycin is more challenging. Rapamycin's three alcohol moieties complicate mono-esterification, which is necessary to minimize hydrolysis of its macrocyclic ester before in vivo generation of the parent drug. Fortunately, site-specific functionalization of only one of rapamycin's alcohols (the 42-OH position, on the cyclohexyl moiety) was achieved by enzymatic esterification using Novozyme 435, yielding rapamycin-aliphatic (*21*). A similar procedure proved ineffective at functionalizing rapamycin with cholesteryl hemisuccinate, presumably due to steric hindrance.

The anti-inflammatory properties of the seven resulting lipophilic prodrugs were investigated in vitro by assessing their ability to reduce cytokine production upon LPS stimulation. Bone marrow cells from C57BL/6 mice were incubated with prodrugs and stimulated with LPS. The malonate prodrugs proved insoluble at therapeutic concentrations and were therefore not analyzed. Of the five remaining prodrugs, all except (+)-JQ1-aliphatic reduced tumor necrosis factor–α (TNFα) production upon LPS stimulation when compared to RPMI control (Fig. 3B and fig. S5A).

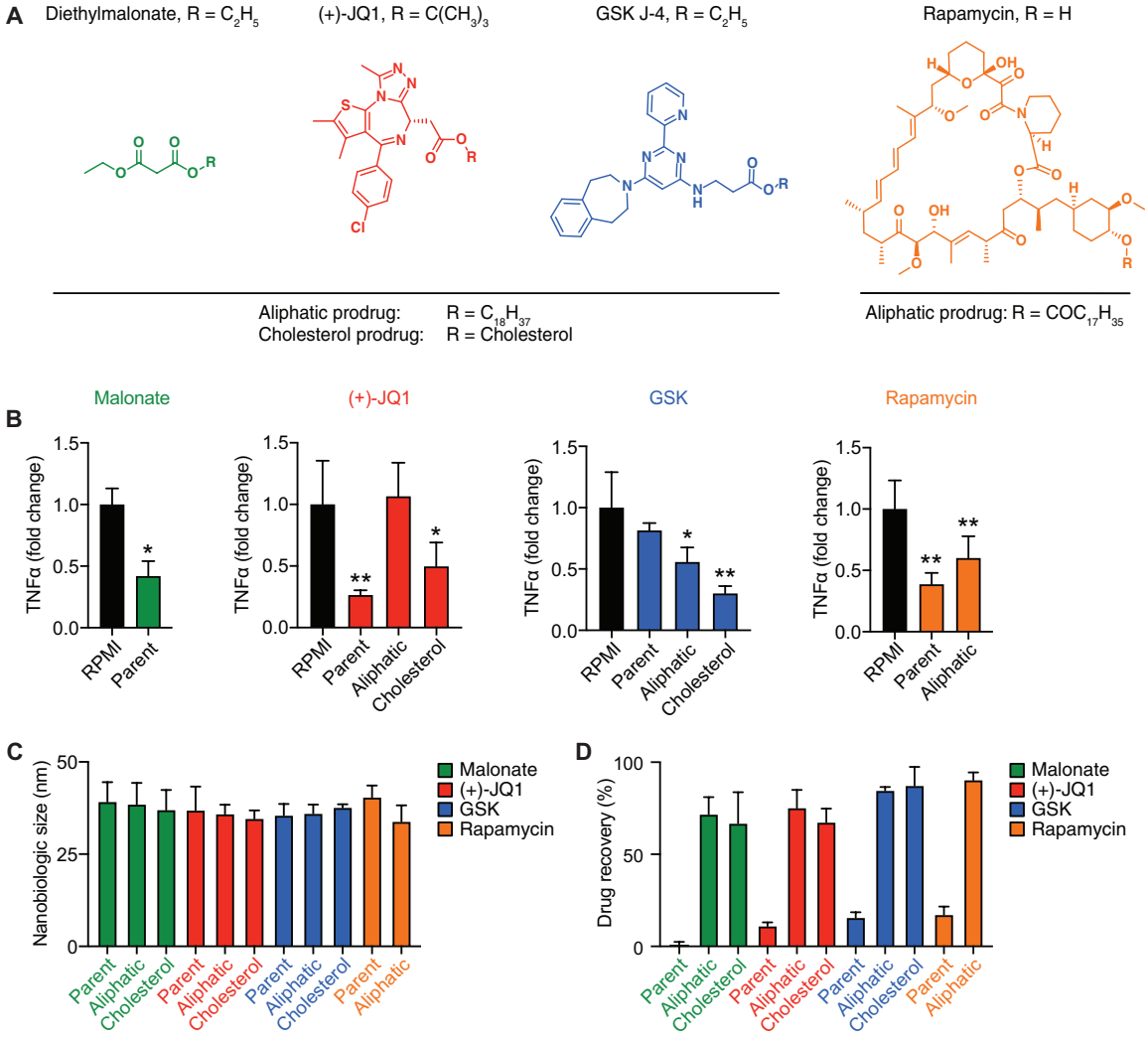

Fig. 3. Establishing a library of nanotherapeutics. (**A**) All drugs were functionalized with either an aliphatic chain or cholesterol using a hydrolyzable ester linkage, except for rapamycin, of which only the aliphatic derivative was synthesized. (**B**) Murine bone marrow cells were incubated with (pro)drugs and stimulated with lipopolysaccharide (LPS; 100 ng/ml) for 24 hours. Subsequently, tumor necrosis factor–α (TNFα) production was measured by enzyme-linked immunosorbent assay; $n = 3$ to 4. (**C**) Size of the nanobiologics as measured by DLS, showing that the type of (pro)drug incorporated has no notable effect on nanobiologic size. The mean of the number average size distribution is displayed; $n = 3$. (**D**) Recoveries of the various (pro)drugs in the nanobiologics as measured by HPLC, defined as the amount of (pro)drug in the nanobiologics divided by the amount used for nanobiologic formulation; $n = 2$. Data in (B) to (D) are represented as means ± SD. $^*P < 0.05$, $^{**}P < 0.01$.

After synthesizing and evaluating the different (pro)drugs, we formulated these compounds in our 35-nm nanobiologic platform, using a 6.5 weight % (wt %) (pro)drug to triglyceride ratio. All formulations were similar in size and dispersity (Fig. 3C and fig. S5B). Furthermore, our prodrug approach resulted in greatly improved incorporation efficiencies compared to the parent drugs, with the recovery of all parent drugs below 20% and all prodrugs above 80%. (Fig. 3D). Unexpectedly, no significant differences were observed between cholesterol and aliphatically functionalized derivatives of the same parent drug. No hydrolytic cleavage of the promoieties was observed over 10 days upon storing the nanobiologics in PBS at 4°C. While some hydrolysis of rapamycin-aliphatic's macrocyclic ester was observed, this was limited to approximately 1.0% per day (fig. S5C). Hydrolysis of unfunctionalized rapamycin in the nanobiologic solution was notably faster but could not be accurately quantified. Together, our results show that, by forming lipophilic prodrugs, a broad variety of therapeutic compounds can be stably incorporated in the 35-nm nanobiologic platform.

Optimizing drug payload of an mTOR-targeting nanobiologic

For the remainder of the study, we focused on rapamycin-aliphatic nanobiologics as the mTOR pathway is a key regulator of innate immune cell function. We first optimized the loading of our rapamycin-aliphatic prodrug (Fig. 4A). We were able to increase the rapamycin-aliphatic payload by a factor 3 without affecting prodrug incorporation efficiency or nanobiologic size and stability (Fig. 4, B and C, see fig. S6 for cryo-TEM image of mTORi-NBs). Further increasing the amount of rapamycin-aliphatic resulted in turbid solutions and increased nanobiologic sizes. We will refer to the mTOR-targeting nanobiologic formulated using 19.5 wt % rapamycin-aliphatic compared to triglycerides as "mTORi-NB." Identical prodrug

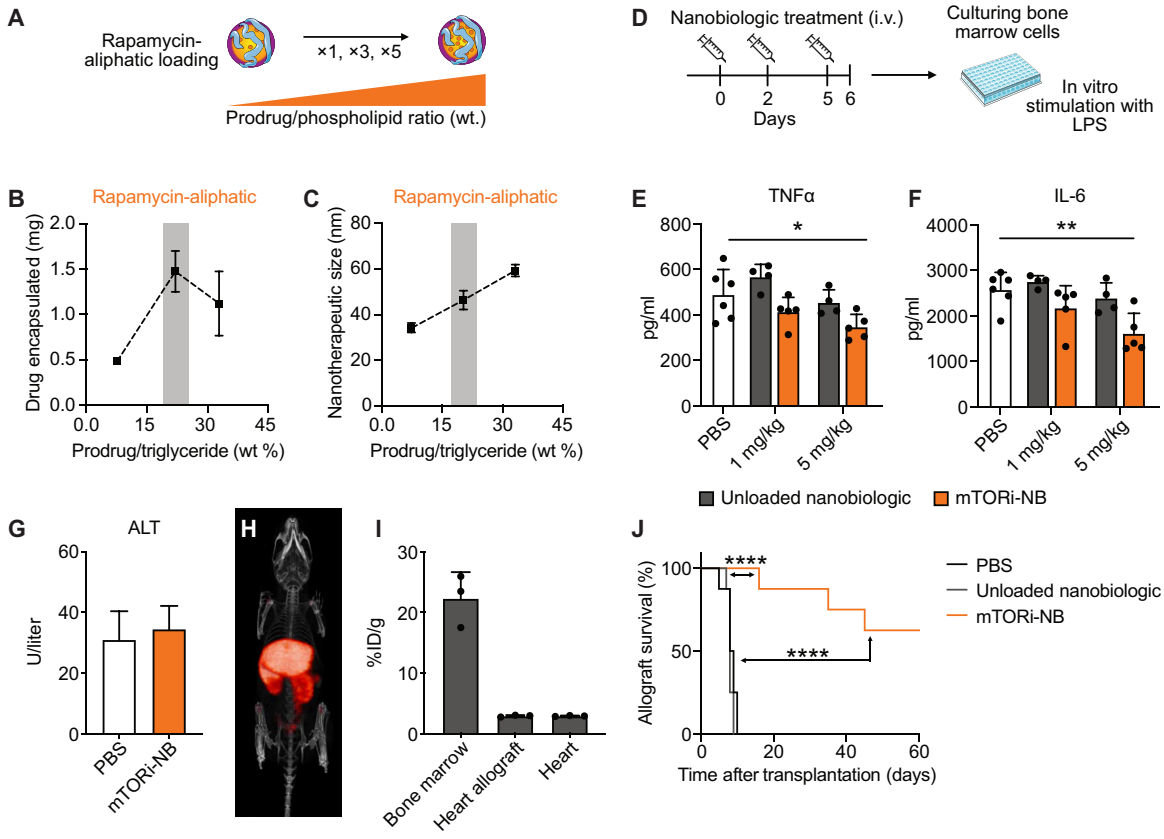

Fig. 4. Using mTORi-nanobiologics to prevent organ rejection in a mouse heart allograft model. (**A** to **C**) Nanobiologics were formulated using 1×, 3×, and 5× a reference amount of rapamycin-aliphatic (equaling prodrug/triglyceride wt % of 6.50, 19.5, and 32.5, respectively), schematically shown in (A). (B) Amount of rapamycin-aliphatic recovered and (C) size of the nanobiologics when formulated using the various amounts of rapamycin-aliphatic; $n = 3$ for each composition. The formulation containing 3× our reference amount of rapamycin-aliphatic (containing ~20 wt % prodrug compared to triglycerides) was chosen as lead candidate and highlighted with a gray bar. This formulation was termed mTORi-NB. (**D** to **G**) C57BL/6 mice were treated with three intravenous injections of either mTORi-NBs at 1.0 or 5.0 mg/kg, a corresponding dose of unloaded nanobiologics, or PBS. Bone marrow cells were harvested on day 6 and stimulated with LPS, schematically shown in (D). (E) TNFα and (F) IL-6 production upon in vitro LPS stimulation; $n = 4$ to 6. (G) Alanine aminotransferase (ALT) blood levels in U/liter; $n = 10$ to 12. (**H** to **J**) C57BL/6 mice received an allogenic heart transplant. (H) Representative maximum intensity projection of a PET/CT scan and (I) organ-specific uptake at 24 hours after ^{89}Zr-labeled mTORi-NB injection. (J) Allograft survival in mice treated with mTORi-NBs, the unloaded 35-nm nanobiologics, or PBS, directly before as well as 2 and 5 days after transplantation. Data are represented as means ± SD. *P* values were calculated using Mann-Whitney *U* tests. For survival analysis, a log-rank test was used. *$P < 0.05$, **$P < 0.01$, ****$P < 0.0001$.

loading experiments using GSK-aliphatic or (+)-JQ1-cholesterol yielded similar results, indicating that a prodrug to triglyceride mass ratio of ~1 to 5 represents an optimum for this nanobiologic platform (fig. S7). To assess their ability to induce immunological tolerance in vivo, we intravenously administered mTORi-NBs to C57BL/6 mice on days 0, 2, and 5 at an equivalent dose of 1.0 or 5.0 mg of rapamycin per kilogram (Fig. 4D). Bone marrow cells were harvested on day 6 and stimulated with LPS in vitro. Cells from mice treated with mTORi-NBs at 5.0 mg/kg displayed a less inflammatory phenotype, as indicated by a reduction in TNFα and interleukin-6 (IL-6) production following LPS stimulation, compared to PBS-treated animals (Fig. 4, E and F). No signs of liver toxicity were observed at this dose (Fig. 4G).

mTOR-targeted nanobiologic immunotherapy prolongs heart allograft survival

We have previously reported a myeloid cell–specific nanotherapy and demonstrated its ability to induce allograft tolerance in a mouse allogeneic heart transplantation model (*2*). Specifically, this treatment reduces glycolysis in macrophages and diminishes the epigenetic modifications underlying inflammatory cytokine production. In turn, these macrophages promote $CD4^+$ regulatory T cell expansion at the expense of alloreactive $CD8^+$ T cell–mediated immunity.

Inspired by these results, we evaluated mTORi-NB immunotherapy's efficacy in the same heart transplantation model. First, we radiolabeled mTORi-NBs with ^{89}Zr to study their biodistribution by PET imaging in mice that underwent heart allograft transplantation. Our results reveal high bone marrow uptake and comparable accumulation between the endogenous and allograft hearts (Fig. 4, H and I). We also evaluated mTORi-NB immunotherapy's ability to prolong allograft survival. Mice were treated with either mTORi-NBs (5.0 mg/kg), nanobiologics containing no drug, or PBS, directly before as well as 2 and 5 days after transplantation. All mice treated with PBS or unloaded nanobiologics had rejected their transplants by day 10, while the allografts of all mTORi-NB–treated animals were still viable 15 days after transplantation (Fig. 4J). Eight weeks after transplantation, 62.5% of the mTORi-NB–treated mice had not rejected the heart allografts, underlining mTORi-NB immunotherapy's potential.

mTOR-targeted nanobiologic immunotherapy is safe in nonhuman primates

To facilitate clinical translation of our nanobiologic platform, we studied mTORi-NB biodistribution and toxicity in two nonhuman primates. ^{89}Zr-labeled mTORi-NBs were intravenously administered, and their in vivo distribution was examined using a fully integrated three-dimensional (3D) PET/magnetic resonance imaging (MRI) protocol that we developed previously (*14*). The PET/MRI protocol allows acquiring high-quality and high-resolution anatomical information while simultaneously detecting ^{89}Zr-labeled nanobiologics by PET imaging with high sensitivity and accuracy. Dynamic scanning revealed that within the first 20 min after

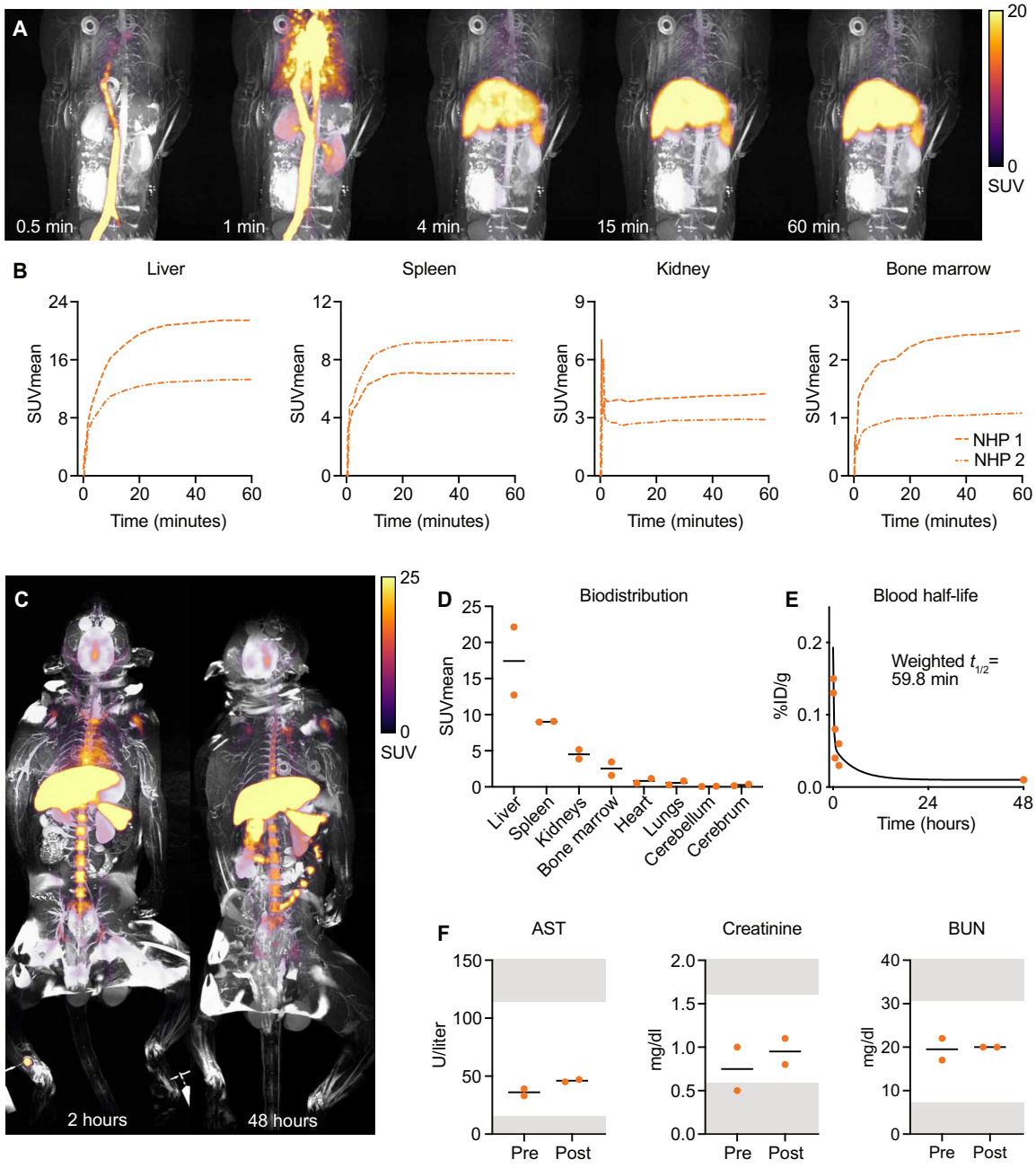

Fig. 5. Biodistribution and safety of mTORi-nanobiologics in nonhuman primates. Two nonhuman primates weighing 5.99 and 10.13 kg were injected with ^{89}Zr-labeled mTORi-NB. (**A**) Representative 3D-rendered images acquired in the first hour after injection using dynamic PET/MR. (**B**) Quantification of ^{89}Zr-labeled mTORi-NB PET signal in liver, spleen, kidneys, and bone marrow. (**C**) Representative whole-body PET/MR images, 2 and 48 hours after injection of ^{89}Zr-labeled mTORi-NBs. (**D**) PET-based quantification of ^{89}Zr-labeled mTORi-NB uptake in various organs at 48 hours after injection. (**E**) Blood pharmacokinetics measured by ex vivo gamma counting of blood samples, as well as the associated weighted blood half-life obtained by fitting the data with a biexponential decay function. (**F**) Aspartate aminotransferase (AST), creatinine, and blood urea nitrogen (BUN) levels before (Pre) and 48 hours after (Post) injection. White areas represent normal ranges for male cynomolgus monkeys (*35*). For all assays, pre- and post-values are comparable. SUV, standardized uptake value.

administration, mTORi-NBs accumulated in the spleen, liver, kidney, and bone marrow (Fig. 5, A and B). Static whole-body PET/MRI was performed 2 and 48 hours after injection, allowing quantification of nanobiologic distribution. At 48 hours after injection, we found the mTORi-NBs mainly accumulated in the liver, spleen, kidney, and bone marrow, while we observed very little activity in the heart, lungs, and brain (Fig. 5, C and D). The weighted blood half-life of a single mTORi-NB dose was 59.8 min, as determined by ex vivo gamma counting of blood samples (Fig. 5E and table S4). Blood chemistry analyses showed no signs of liver or kidney damage 48 hours after injection (Fig. 5F). These results indicate that the in vivo behavior and biocompatibility of mTORi-NBs are preserved across species.

DISCUSSION

In this study, we present a modular approach for producing nanotherapeutics that efficiently engage the innate immune system. These nanotherapeutics are based on highly biocompatible nanobiologics that are formulated from natural molecular building blocks, namely, phospholipids, other fatty molecules, and apoA-I, using a simple, fast, and reproducible microfluidic formulation process (*22*). In mouse studies, we found that the 35-nm-sized nanobiologics rapidly accumulate in hematopoietic organs and display a strong affinity for myeloid cells and their progenitors.

Our prodrug strategy allows efficient and stable nanobiologic loading with a broad variety of drugs. All prodrugs were incorporated with similar efficiencies without affecting nanobiologic size or dispersity. In other words, instead of pursuing conventional drug formulation strategies focused on modifying the nanocarrier, we chemically modified the therapeutic payload to be inherently compatible with our optimized nanobiologic platform. Therefore, our combined nanobiologic and prodrug approach allows producing nanotherapeutics for targeting myeloid (progenitor) cells in a modular, yet highly reproducible fashion.

After showing that a variety of drugs can be straightforwardly incorporated in our nanobiologic platform, we demonstrated its high propensity for myeloid cell uptake. We optimized the loading of a rapamycin prodrug in nanobiologics to yield mTORi-NBs. mTORi-NBs therapy significantly promoted organ transplant acceptance in a murine model of heart allograft transplantation without the need for chronic immunosuppression. In mice treated with mTORi-NBs, more than half of the allografts survived over 60 days, whereas all allografts in animals treated with PBS or unloaded nanobiologics rejected within 10 days after transplantation. We observed a similar biodistribution of mTORi-NBs in nonhuman primates as observed in mice, with no signs of toxicity in either species. These results show that nanobiologics' favorable in vivo features are preserved across species. Nanobiologics enhance the bioavailability for innate immune cells, which is concurrently expected to reduce systemic side effects. In the case of rapamycin, insulin resistance and impaired wound healing are avoided (*23*, *24*).

In future research, we will focus on expanding our prodrug library with additional therapeutic agents as well as different promoieties and biocleavable groups. The relation between promoiety structure and prodrug in vivo behavior will be of special interest. Although our current study used drugs that induce immunological tolerance, similar platforms can be used to initiate other types of innate immune responses (*12*). Producing these immunostimulatory nanotherapeutics in a modular fashion could greatly benefit treating a broad variety of diseases, including cancer or coronavirus disease 2019 (COVID-19) (*25*, *26*). We expect our modular approach to greatly benefit from current developments in high-throughput screening and machine learning, further accelerating nanotherapeutic development and clinical translation (*27*, *28*). Clinical translation is further facilitated by the ease with which our microfluidic nanobiologic formulation technology can be scaled up (*22*). apoA-I has been produced (in sufficient amounts) for safe application in humans (*29*–*32*).

In summary, we developed a robust and fully modular approach toward producing nanotherapeutics with a high propensity to accumulate in hematopoietic organs where they target myeloid cells. The latter facilitates efficient modulation of the innate immune response, which we demonstrated in vitro and in vivo in a heart allograft mouse model. Through easily scalable production and safe application in nonhuman primate models, we have demonstrated the clinical translatability of our nanobiologic platform.

MATERIALS AND METHODS

Materials

All chemicals were purchased from Sigma-Aldrich, Medchem Express, or Selleckchem, except p-SCN-Bn-Defereoxamine that was obtained from macrocyclics. PES (polyethersulfone) syringe filters were obtained from CELLTREAT. A BS-8000 model microfluidic pump from Braintree Scientific Inc. was used to formulate the nanobiologics in combination with Zeonor herringbone mixers from microfluidic ChipShop (product code: 10000076). Particles were purified using a 100-kDa MWCO 20-ml Vivaspin centrifugal filter. Dialysis bags were from Thermo Fisher Scientific (product no. 66383). The apoA-1 protein was purified in house using a combination of ultracentrifugation and precipitation in chloroform/methanol. DLS and zeta potential measurements were performed on a Brookhaven Instruments Corporation ZetaPALS analyzer. ^{1}H and ^{13}C nuclear MR samples were analyzed using a Bruker 600 ultrashield magnet connected to a Bruker advance 600 console, and data were processed using TopSpin version 3.5 pl 7. Quantitative analysis of all drugs, except diethyl malonate and its derivatives, was performed by high-performance liquid chromatography (HPLC) using a Shimadzu UFLC apparatus equipped with either a C_{18} or CN column. Acetonitrile and water (each with 0.1% trifluoroacetic acid) were used as mobile phase, and compounds were detected with an SPD-M20a diode array detector. Diethyl malonate was analyzed using an Agilent Technologies 5977B MSD 7890B gas chromatography–mass spectrometry (GC-MS), equipped with an HP5MS 30-m, 0.25-mm, 0.25-μm column. Aliphatic and cholesterol-derivatized malonate were analyzed with a Waters ACQUITY UPC2 SFC (supercritical fluid)–MS using an isopropanol/water mixture as a mobile phase and a 1-aminoantracene column. Radiolabeling of the nanoparticles was performed using a procedure previously reported by us (*13*, *22*). Elemental analysis was outsourced to Galbraith Laboratories.

Formulating the 35-nm nanobiologics

From stock solutions (10 mg/ml) in chloroform, POPC (250 μl), PHPC (65 μl), cholesterol (15 μl), tricaprylin (1000 μl), and optional (pro)drug (65 μl) were combined in a 20-ml vial and dried under vacuum. The resulting film was redissolved in an acetonitrile/methanol mixture (95:5%, 3-ml total volume). Separately, a solution of apoA-I

protein in PBS (24 ml, 0.1 mg/ml) was prepared. Using a microfluidic setup, both solutions were simultaneously injected into a herringbone mixer, with a flow rate of 0.75 ml/min for the lipid solution and a rate of 6 ml/min for the apoA-I solution. The obtained solution was concentrated by centrifugal filtration using a 100 MWCO Vivaspin tube at 4000 rpm to obtain a volume of 5 ml. PBS (5 ml) was added and the solution was concentrated to 5 ml; this was repeated twice. The washed solution was concentrated to approximately 3 ml and filtered through a 0.22-μm PES syringe filter to obtain the finished nanobiologics. To obtain nanobiologics for fluorescence-activated cell sorting (FACS) measurements, 3,3′-dioactadecyloxacarbocyanine perchlorate [$DIOC_{18}$(3); 0.25 mg] was added to the acetonitrile solution.

Radiolabeling the nanobiologics

To obtain nanobiologics for ^{89}Zr labeling, the nanobiologic solutions were adjusted to pH 8 using a carbonate buffer and p-SCN-Bn-DFO (2 eq. per apoA-I) was added as a concentrated solution in dimethyl sulfoxide (no more than 5 volume %). The mixture was incubated at 37°C for 2 hours, and the solution was washed three times with water in a 100-kDa Vivaspin tube. A solution of ^{89}Zr oxalate (1 M aqueous oxalic acid) was neutralized using sodium carbonate (1 M in water) until a pH between 6.8 and 7.4 was reached. The ^{89}Zr solution was added to the DFO-containing nanobiologics and incubated at 37°C using a thermomixer (600 rpm) for 30 to 60 min. The resulting solution was purified by washing three times with water in a 10-kDa Vivaspin tube. The radiolabeled nanobiologics' radiochemical purity was typically over 95%, as assessed by size exclusion chromatography radio-HPLC.

Determination of nanobiologic size and dispersity by DLS

An aliquot (10 μl) of the final nanobiologic solution was dissolved in PBS (1 ml), filtered through a 0.22-μm PES syringe filter, and analyzed by DLS. Values are reported as the mean of the number average size distribution.

Determining drug recovery and hydrolysis

(Pro)drug recovery and hydrolysis were determined by drying an aliquot (200 μl) of the nanobiologics under vacuum and dissolving the residue in acetonitrile (600 μl) by sonicating for 5 min. The suspension was centrifuged to precipitate any solids, and the remaining solution was analyzed by HPLC using a PDA (photodiode array) detector, except for nanobiologics containing diethylmalonate, which were analyzed by GC-MS, and those containing malonate prodrugs, which were analyzed using SFC-MS.

Determining model drug release by dialysis in FBS

To compare the stability of the nanobiologics under in vivo–like conditions, the nanoparticles were dialyzed against FBS at 37°C. The nanobiologic solution (0.5 ml) was placed in a 10-kDa MWCO dialysis bag and suspended in FBS (45 ml) at 37°C. At predetermined time points (0, 15, 30, 60, 120, and 360 min after starting the experiment), an aliquot (50 μl) was taken from the dialysis bag and analyzed by HPLC as explained above. Experiments were performed in duplicate using the same batch of nanobiologics. The obtained kinetic data were fitted using a biexponential decay after testing for outliers (none were identified by Prism's ROUT method using $Q = 1\%$) and subsequently normalized using the y-axis intercept of the fit.

Cryogenic transmission electron microscopy

Vitrified thin films for cryo-TEM analysis were prepared using an automated vitrification robot (FEI Vitrobot Mark IV) by plunge vitrification in liquid ethane. Before vitrification, a 200-mesh copper grid covered with a Quantifoil R 2/2 holey carbon film (Quantifoil Micro Tools GmbH) was surface plasma–treated for 40 s using a Cressington 208 carbon coater. Cryo-TEM imaging was carried out on the cryoTITAN (Thermo Fisher Scientific, previously FEI), equipped with a field emission gun, a post-column Gatan imaging filter (model 2002), and a post-GIF 2k × 2k Gatan charge-coupled device camera (model 794). The microscope was operated at 300-kV acceleration voltage in bright-field TEM mode with zero-loss energy filtering at a nominal magnification of ×24,000 and a dose rate of 11.8 $e^{-}/Å^{2}{\cdot}s$ with a 1^{-s} image acquisition time.

Animal models

Female C57BL/6 and BALB/c mice were purchased from The Jackson Laboratory. For nonhuman primate studies, two male cynomolgus monkeys (*Macaca fascicularis*) were used. All animals were cohoused in climate-controlled conditions with 12-hour light-dark cycles and provided water ad libitum. Mice were fed a standard chow diet. Nonhuman primates were fed Teklad Global 20% Protein Primate Diet. Animal care and experimental procedures were based on approved institutional protocols from the Icahn School of Medicine at Mount Sinai.

Pharmacokinetics in mice and nonhuman primates

To determine the in vivo half-life of the nanobiologics, ^{89}Zr-labeled nanobiologics (106.4 ± 30.28 μCi) were intravenously injected in C57BL/6 mice. Blood was drawn at 1, 5, 15, and 30 min and 1, 2, 6, 12, and 24 hours after injection. Two nonhuman primates weighing 10.13 and 5.99 kg were injected with 2249 μCi and 1274 μCi ^{89}Zr-labeled mTORi-NBs, respectively. Blood was drawn at 5, 30, and 90 min and 48 hours after injection. Blood samples were weighed and gamma-counted using a Wizard^2 2480 automatic gamma counter (PerkinElmer, Waltham, MA). Values were corrected for radioactive decay and expressed as a percentage of injected dose per gram of blood (%ID/g). Mouse and nonhuman primate data were fitted with a biexponential decay function. Weighted half-life was defined as follows: (% fast × $t_{1/2}$ fast + % slow × $t_{1/2}$ slow)/100.

Biodistribution studies

C57BL/6 mice were sacrificed 24 hours after injection of ^{89}Zr-labeled nanobiologics and perfused with PBS (20 ml). Tissues of interest were harvested, weighed, and gamma-counted using a Wizard^2 2480 automatic gamma counter (PerkinElmer, Waltham, MA). Values were corrected for decay and expressed as a percentage of injected dose per gram of tissue (%ID/g).

PET/CT imaging of nanobiologic biodistribution in mice

^{89}Zr-labeled nanobiologics (106.4 ± 30.28 μCi) were intravenously injected in C57BL/6 mice. Twenty-four hours later, mice were anesthetized using 1.0% isoflurane in O_2 at a flow rate of ~1.0 liter/min. PET/CT scans were performed using a Mediso nanoScan PET/CT (Mediso, Budapest, Hungary). A whole-body CT scan was performed (energy, 50 kVp; current, 180 μAs; isotropic voxel size, 0.25 mm) followed by a 20-min PET scan. Reconstruction was performed with attenuation correction using the TeraTomo 3D reconstruction algorithm from the Mediso Nucline software. The coincidences

were filtered with an energy window between 400 and 600 keV. The voxel size was isotropic with 0.4-mm width, and the reconstruction was applied for four full iterations, six subsets per iteration.

Determining cellular uptake of $DiOC_{18}$-labeled or BODIPY model drug-loaded nanobiologics by flow cytometry

To study cellular specificity, C57BL/6 mice were injected with nanobiologics containing highly lipophilic $DiOC_{18}$, dosed at 0.6 mg of $DiOC_{18}$ per kilogram of mice. Similarly, (pro)drugs' bone marrow delivery was qualitatively investigated by injecting mice with either bare BODIPY FL carboxylic acid, or nanobiologics loaded with aliphatic or cholesteryl ester derivatives thereof. Specifically, bare BODIPY FL carboxylic acid was injected at 0.1, 0.5, and 2.5 mg/kg. In addition, separate groups of animals were injected with constant amounts of nanobiologics, loaded with differing amounts of BODIPY prodrug. Nanobiologics containing 0.65, 3.25, or 16.25 wt % BODIPY (model prodrug) compared to tricaprylin (see table S2) were injected at 0.1, 0.5, and 2.5 mg/kg, respectively. Animals were euthanized 24 hours later, and their blood was collected through cardiac puncture. Blood samples were stored in EDTA-coated tubes. The animals were subsequently perfused with cold PBS (20 ml). Femurs and spleen were collected and stored in PBS. Bone marrow cells were flushed out of femurs and strained through a 70-μm strainer. Spleens were fragmented and meshed through a 70-μm strainer. Blood, bone marrow, and spleen samples were incubated with lysis buffer and washed with FACS buffer (Dulbecco's PBS complemented with 1% FBS, 1 mM EDTA, 0.5% bovine serum albumin, and 0.1% NaN_3).

Single-cell suspensions were incubated with anti-CD115 (clone AFS98), anti-Ly6C (clone Al-21), anti-Ly6G (clone 1A8), anti-CD11b (clone M1/70), anti-CD19 (clone 1D3), and anti-CD90.2 (clone 53-2.1). To determine uptake in stem and progenitor cells, bone marrow cells were stained with anti-CD48 (clone HM48-1), anti-CD150 (clone TC15-12F12.2), anti-CD135 (clone A2F10), anti-CD117 (c-Kit) (clone 2B8), anti–Sca-1 (Ly6-A/E) (clone E13-161.7), anti-CD16/32 (clone 93), anti-CD34 (clone RAM34), and a lineage cocktail containing anti-CD3ε (clone 500A2), anti-CD11b (clone M1/70), anti-CD45R/B220 (clone RA3-6B2), anti–Ly-76 (clone TER-119), and anti-Ly6G/Ly6C (clone RB6-8C5). Antibodies were purchased from BioLegend, BD Biosciences, and eBioscience. Data were acquired on a BD LSRFortessa (BD Biosciences). $DiOC_{18}$ and BODIPY signals were detected in the fluorescein isothiocyanate (FITC) channel. Data were analyzed using FlowJo v10.4.0 (Tree Star).

In vivo nanobiologic treatment

Mice were treated directly before as well as 2 and 5 days after transplantation with mTORi-NBs (5.0 mg/kg), an equivalent dose of unloaded nanobiologics, or PBS through lateral tail vein injection. mTORi-NBs were dosed at 1- or 5-mg effective amount of rapamycin per kilogram of animal. Nonhuman primates were treated once with mTORi-NBs, intravenously, at 0.15 mg/kg. This is the equivalent of the 1.0 mg/kg dose in mice, corrected for body surface area (*33*).

Assessing in vitro (pro)drug efficacy

Bone marrow cells were harvested from tibias and femurs of naïve C57BL/6 mice or C57BL/6 mice treated with nanobiologics. Cells were filtered through a 70-μm strainer, incubated with lysis buffer, and washed with cold PBS. Cells were resuspended in complete medium (RPMI 1640 medium supplemented with 10% FBS and 1% penicillin-streptomycin, 1% L-glutamine solution, 1% minimum essential medium nonessential amino acids, and 1% Hepes buffer) at 0.75×10^6 cells/ml. Cells were seeded at 750,000 cells per well in a 24-well plate. Cells of naïve mice were incubated with (pro)drugs and left to adhere for 1 hour (GSK and rapamycin) or 24 hours [(+)-JQ1] at 37°C. We tested malonate at a concentration of 2.5 mM, (+)-JQ1 and its prodrugs at 50 nM, GSK and its prodrugs at 10 μM, and rapamycin and its prodrug at 40 nM. Cells were stimulated with LPS at a concentration of 100 ng/ml for another 24 hours. Cells of mice treated with nanobiologics were left to adhere for 1 hour at 37°C. Cells were stimulated with LPS at a concentration of 100 ng/ml for another 24 hours. The supernatant was collected and stored at −80°C until further analysis.

Quantification of cytokines in the cell culture supernatant

Cytokine production was determined in supernatants using commercial enzyme-linked immunosorbent assay kits for murine TNFα and IL-6 (Invitrogen) following the instructions of the manufacturer.

Cell viability assay

Bone marrow cells were harvested as described above and plated at 50,000 cells per well in a 96-well plate. Cells were incubated with (pro)drugs for 24 hours. We tested malonate at a concentration of 2.5 mM, (+)-JQ1 and its prodrugs at 50 nM, GSK and its prodrugs at 10 μM, and rapamycin and its prodrug at 40 nM. The CellTiter-Glo Luminescent Cell Viability Assay (Promega) was performed following the instructions of the manufacturer.

Murine heart transplantation and allograft monitoring

Hearts of BALB/c mice were transplanted as fully vascularized heterotopic grafts into C57BL/6 mice as previously described (*34*). Briefly, hearts were transplanted into the peritoneal cavities of the recipients by establishing an end-to-side anastomosis between the donor and recipient aortae and end-to-side anastomosis between the donor pulmonary trunk and the recipient inferior vena cava. To determine cardiac allograft survival, transplanted hearts were checked two to three times per week by ultrasound. Hearts were imaged using a Vevo 2100 Imaging System (FUJIFILM VisualSonics Inc.) with an MS-400 transducer (30 MHz) in B-mode. Rejection was defined as the complete absence of cardiac contraction. Graft survival among groups was plotted using Kaplan-Meier survival curves. Statistical significance was calculated using log-rank tests.

In vivo PET/MRI of nonhuman primates

PET and MR images were acquired on a combined 3T PET/MRI system (Biograph mMR, Siemens Healthineers). After an overnight fast, animals were anesthetized with ketamine (5.0 mg/kg) and dexmedetomidine (0.0075 to 0.015 mg/kg), and blood was collected from the femoral vein. The animals were injected with ^{89}Zr-labeled mTORi-NBs. Dynamic PET imaging was performed during the first 60 min after infusion, while static whole-body PET scans were performed starting at 1 and 48 hours after injection. During imaging, blood was collected at 5, 30, and 90 min, and 48 hours after injection, to determine the nanobiologics' pharmacokinetics.

The dynamic PET bed was positioned to capture the kidneys, liver, spleen, and lumbar vertebrae. Static whole-body PET images were acquired from the cranium to the pelvis, using four consecutive bed positions.

During dynamic imaging, MR parameters were as follows: acquisition plane, coronal; repetition time, 1000 ms; echo time, 79 ms; number of slices, 144; number of averages, 4; spatial resolution, 0.5 mm × 0.5 mm × 1.0 mm; and acquisition duration, 42 min and 42 s. For whole-body imaging starting at 1 hour after injection, MR parameters were as follows: acquisition plane, coronal; repetition time, 1000 ms; echo time, 79 ms; number of slices, 160; number of averages, 1.4; spatial resolution, 0.6 mm × 0.6 mm × 1.0 mm; and acquisition duration, 14 min and 56 s per bed. For whole-body imaging starting at 48 hours after injection, MR parameters were as follows: acquisition plane, coronal; repetition time, 1000 ms; echo time, 79 ms; number of slices, 224; number of averages, 2; spatial resolution of 0.6 mm × 0.6 mm × 1.0 mm; acquisition duration, 29 min and 56 s per bed.

Whole-body MR images from each bed were automatically collated together with a scanner. After acquisition, PET raw data from each bed were reconstructed and collated together offline using the Siemens proprietary e7tools with an ordered subset expectation maximization (OSEM) algorithm with point spread function (PSF) correction. A dual-compartment (soft tissue and air) attenuation map was used for attenuation.

Imaging-based analysis of the nanobiologics' biodistribution in nonhuman primates

Image analysis was performed using Osirix MD, version 11.0. Whole-body MR images were fused with PET images and analyzed in a coronal plane. Regions of interest (ROIs) were drawn on various tissues. The spleen, liver, kidneys, lungs, heart, cerebellum, and cerebrum were traced in their entirety, and bone marrow uptake was assessed using three vertebrae in the lumbar spine. Mean standardized uptake values (SUVs) were calculated for each ROI. Subsequently, ^{89}Zr-labeled mTORi-NB uptake of each organ was expressed as the average of all mean SUV values per organ.

Blood chemistry

Nonhuman primate and mouse serum were collected, and blood chemistry analysis was performed by IDEXX BioAnalytics.

SUPPLEMENTARY MATERIALS

Supplementary material for this article is available at http://advances.sciencemag.org/cgi/content/full/7/10/eabe7853/DC1

View/request a protocol for this paper from *Bio-protocol*.

REFERENCES AND NOTES

1. W. J. M. Mulder, J. Ochando, L. A. B. Joosten, Z. A. Fayad, M. G. Netea, Therapeutic targeting of trained immunity. *Nat. Rev. Drug Discov.* **18**, 553–566 (2019).
2. M. S. Braza, M. M. T. van Leent, M. Lameijer, B. L. Sanchez-Gaytan, R. J. W. Arts, C. Pérez-Medina, P. Conde, M. R. Garcia, M. Gonzalez-Perez, M. Brahmachary, F. Fay, E. Kluza, S. Kossatz, R. J. Dress, F. Salem, A. Rialdi, T. Reiner, P. Boros, G. J. Strijkers, C. C. Calcagno, F. Ginhoux, I. Marazzi, E. Lutgens, G. A. F. Nicolaes, C. Weber, F. K. Swirski, M. Nahrendorf, E. A. Fisher, R. Duivenvoorden, Z. A. Fayad, M. G. Netea, W. J. M. Mulder, J. Ochando, Inhibiting inflammation with myeloid cell-specific nanobiologics promotes organ transplant acceptance. *Immunity* **49**, 819–828.e6 (2018).
3. S. Saeed, J. Quintin, H. H. D. Kerstens, N. A. Rao, A. Aghajanirefah, F. Matarese, S.-C. Cheng, J. Ratter, K. Berentsen, M. A. van der Ent, N. Sharifi, E. M. Janssen-Megens, M. T. Huurne, A. Mandoli, T. van Schaik, A. Ng, F. Burden, K. Downes, M. Frontini, V. Kumar, E. J. Giamarellos-Bourboulis, W. H. Ouwehand, J. W. M. van der Meer, L. A. B. Joosten, C. Wijmenga, J. H. A. Martens, R. J. Xavier, C. Logie, M. G. Netea, H. G. Stunnenberg, Epigenetic programming of monocyte-to-macrophage differentiation and trained innate immunity. *Science* **345**, 1251086 (2014).
4. Y. Zhao, F. Fay, S. Hak, J. M. Perez-Aguilar, B. L. Sanchez-Gaytan, B. Goode, R. Duivenvoorden, C. de Lange Davies, A. Bjørkøy, H. Weinstein, Z. A. Fayad, C. Pérez-Medina, W. J. M. Mulder, Augmenting drug–carrier compatibility improves tumour nanotherapy efficacy. *Nat. Commun.* **7**, 11221 (2016).
5. R. Kuai, D. Li, Y. E. Chen, J. J. Moon, A. Schwendeman, High-density lipoproteins: Nature's multifunctional nanoparticles. *ACS Nano* **10**, 3015–3041 (2016).
6. I. F. Usynin, A. N. Dudarev, A. Y. Gorodetskaya, S. M. Miroshnichenko, T. A. Tkachenko, V. I. Tkachenko, Apolipoprotein A-I stimulates cell proliferation in bone marrow cell culture. *Bull. Exp. Biol. Med.* **164**, 308–311 (2018).
7. J. Tang, S. Baxter, A. Menon, A. Alaarg, B. L. Sanchez-Gaytan, F. Fay, Y. Zhao, M. Ouimet, M. S. Braza, V. A. Longo, D. Abdel-Atti, R. Duivenvoorden, C. Calcagno, G. Storm, S. Tsimikas, K. J. Moore, F. K. Swirski, M. Nahrendorf, E. A. Fisher, C. Pérez-Medina, Z. A. Fayad, T. Reiner, W. J. M. Mulder, Immune cell screening of a nanoparticle library improves atherosclerosis therapy. *Proc. Natl. Acad. Sci. U.S.A.* **113**, E6731–E6740 (2016).
8. L. Coderch, J. Fonollosa, M. De Pera, J. Estelrich, A. D. La Maza, J. L. Parra, Influence of cholesterol on liposome fluidity by EPR: Relationship with percutaneous absorption. *J. Control. Release* **68**, 85–95 (2000).
9. M.-L. Briuglia, C. Rotella, A. McFarlane, D. A. Lamprou, Influence of cholesterol on liposome stability and on in vitro drug release. *Drug Deliv. Transl. Res.* **5**, 231–242 (2015).
10. G. Le Roux, H. Moche, A. Nieto, J.-P. Benoit, F. Nesslany, F. Lagarce, Cytotoxicity and genotoxicity of lipid nanocapsules. *Toxicol. Vitr.* **41**, 189–199 (2017).
11. A. Wretlind, The toxicity of low-molecular triglycerides. *Acta Physiol. Scand.* **40**, 338–343 (1957).
12. B. Priem, M. M. T. van Leent, A. J. P. Teunissen, A. M. Sofias, V. P. Mourits, L. Willemsen, E. D. Klein, R. S. Oosterwijk, A. E. Meerwaldt, J. Munitz, G. Prévot, A. V. Verschuur, S. A. Nauta, E. M. van Leeuwen, E. L. Fisher, K. A. M. de Jong, Y. Zhao, Y. C. Toner, G. Soultanidis, C. Calcagno, P. H. H. Bomans, H. Friedrich, N. Sommerdijk, T. Reiner, R. Duivenvoorden, E. Zupančič, J. S. Di Martino, E. Kluza, M. Rashidian, H. L. Ploegh, R. M. Dijkhuizen, S. Hak, C. Pérez-Medina, J. J. Bravo-Cordero, M. P. J. de Winther, L. A. B. Joosten, A. van Elsas, Z. A. Fayad, A. Rialdi, D. Torre, E. Guccione, J. Ochando, M. G. Netea, A. W. Griffioen, W. J. M. Mulder, Trained immunity-promoting nanobiologics suppress tumor growth and potentiate checkpoint blockade immunotherapy. *Cell* **183**, 786–801 (2020).
13. C. Pérez-Medina, J. Tang, D. Abdel-Atti, B. Hogstad, M. Merad, E. A. Fisher, Z. A. Fayad, J. S. Lewis, W. J. M. Mulder, T. Reiner, PET imaging of tumor-associated macrophages with ^{89}Zr-labeled high-density lipoprotein nanoparticles. *J. Nucl. Med.* **56**, 1272–1277 (2015).
14. M. Lameijer, T. Binderup, M. M. T. van Leent, M. L. Senders, F. Fay, J. Malkus, B. L. Sanchez-Gaytan, A. J. P. Teunissen, N. Karakatsanis, P. Robson, X. Zhou, Y. Ye, G. Wojtkiewicz, J. Tang, T. T. P. Seijkens, J. Kroon, E. S. G. Stroes, A. Kjaer, J. Ochando, T. Reiner, C. Pérez-Medina, C. Calcagno, E. A. Fisher, B. Zhang, R. E. Temel, F. K. Swirski, M. Nahrendorf, Z. A. Fayad, E. Lutgens, W. J. M. Mulder, R. Duivenvoorden, Efficacy and safety assessment of a TRAF6-targeted nanoimmunotherapy in atherosclerotic mice and non-human primates. *Nat. Biomed. Eng.* **2**, 279–292 (2018).
15. C. Zheng, M. Aikawa, High-density lipoproteins: From function to therapy. *J. Am. Coll. Cardiol.* **60**, 2380–2383 (2012).
16. A. B. Descalzo, P. Ashokkumar, Z. Shen, K. Rurack, On the aggregation behaviour and spectroscopic properties of alkylated and annelated boron-dipyrromethene (BODIPY) dyes in aqueous solution. *ChemPhotoChem* **4**, 120–131 (2020).
17. E. L. Mills, B. Kelly, A. Logan, A. S. H. Costa, M. Varma, C. E. Bryant, P. Tourlomousis, J. H. M. Däbritz, E. Gottlieb, I. Latorre, S. C. Corr, G. McManus, D. Ryan, H. T. Jacobs, M. Szibor, R. J. Xavier, T. Braun, C. Frezza, M. P. Murphy, L. A. O'Neill, Succinate dehydrogenase supports metabolic repurposing of mitochondria to drive inflammatory macrophages. *Cell* **167**, 457–470.e13 (2016).
18. P. Filippakopoulos, J. Qi, S. Picaud, Y. Shen, W. B. Smith, O. Fedorov, E. M. Morse, T. Keates, T. T. Hickman, I. Felletar, M. Philpott, S. Munro, M. R. McKeown, Y. Wang, A. L. Christie, N. West, M. J. Cameron, B. Schwartz, T. D. Heightman, N. L. Thangue, C. A. French, O. Wiest, A. L. Kung, S. Knapp, J. E. Bradner, Selective inhibition of BET bromodomains. *Nature* **468**, 1067–1073 (2010).
19. L. Kruidenier, C.-w. Chung, Z. Cheng, J. Liddle, K. H. Che, G. Joberty, M. Bantscheff, C. Bountra, A. Bridges, H. Diallo, D. Eberhard, S. Hutchinson, E. Jones, R. Katso, M. Leveridge, P. K. Mander, J. Mosley, C. Ramirez-Molina, P. Rowland, C. J. Schofield, R. J. Sheppard, J. E. Smith, C. Swales, R. Tanner, P. Thomas, A. Tumber, G. Drewes, U. Oppermann, D. J. Patel, K. Lee, D. M. Wilson, A selective jumonji H3K27 demethylase inhibitor modulates the proinflammatory macrophage response. *Nature* **488**, 404–408 (2012).
20. S.-C. Cheng, J. Quintin, R. A. Cramer, K. M. Shepardson, S. Saeed, V. Kumar, E. J. Giamarellos-Bourboulis, J. H. A. Martens, N. A. Rao, A. Aghajanirefah, G. R. Manjeri, Y. Li, D. C. Ifrim, R. J. W. Arts, B. M. J. W. van der Veer, P. M. T. Deen, C. Logie, L. A. O'Neill, P. Willems, F. L. van de Veerdonk, J. W. M. van der Meer, A. Ng, L. A. B. Joosten, C. Wijmenga, H. G. Stunnenberg, R. J. Xavier, M. G. Netea, MTOR- and HIF-1α-mediated aerobic glycolysis as metabolic basis for trained immunity. *Science* **345**, 1250684 (2014).
21. J. Gu, M. E. Ruppen, P. Cai, Lipase-catalyzed regioselective esterification of rapamycin: Synthesis of temsirolimus (CCI-779). *Org. Lett.* **7**, 3945–3948 (2005).
22. T. Binderup, R. Duivenvoorden, F. Fay, M. M. T. van Leent, J. Malkus, S. Baxter, S. Ishino, Y. Zhao, B. Sanchez-Gaytan, A. J. P. Teunissen, Y. C. A. Frederico, J. Tang, G. Carlucci,

S. Lyashchenko, C. Calcagno, N. Karakatsanis, G. Soultanidis, M. L. Senders, P. M. Robson, V. Mani, S. Ramachandran, M. E. Lobatto, B. A. Hutten, J. F. Granada, T. Reiner, F. K. Swirski, M. Nahrendorf, A. Kjaer, E. A. Fisher, Z. A. Fayad, C. Pérez-Medina, W. J. M. Mulder, Imaging-assisted nanoimmunotherapy for atherosclerosis in multiple species. *Sci. Transl. Med.* **11**, eaaw7736 (2019).
23. A. B. Salmon, About-face on the metabolic side effects of rapamycin. *Oncotarget* **6**, 2585–2586 (2015).
24. S. C. Johnson, M. Kaeberlein, Rapamycin in aging and disease: Maximizing efficacy while minimizing side effects. *Oncotarget* **7**, 44876–44878 (2016).
25. L. A. J. O'Neill, M. G. Netea, BCG-induced trained immunity: Can it offer protection against COVID-19? *Nat. Rev. Immunol.* **20**, 335–337 (2020).
26. A. Mantovani, M. G. Netea, Trained innate immunity, epigenetics, and Covid-19. *N. Engl. J. Med.* **383**, 1078–1080 (2020).
27. G. Yamankurt, E. J. Berns, A. Xue, A. Lee, N. Bagheri, M. Mrksich, C. A. Mirkin, Exploration of the nanomedicine-design space with high-throughput screening and machine learning. *Nat. Biomed. Eng.* **3**, 318–327 (2019).
28. K. Paunovska, D. Loughrey, C. D. Sago, R. Langer, J. E. Dahlman, Using large datasets to understand nanotechnology. *Adv. Mater.* **31**, e1902798 (2019).
29. P. G. Lerch, V. Förtsch, G. Hodler, R. Bolli, Production and characterization of a reconstituted high density lipoprotein for therapeutic applications. *Vox Sang.* **71**, 155–164 (1996).
30. C. L. Nykiforuk, Y. Shen, E. W. Murray, J. G. Boothe, D. Busseuil, E. Rhéaume, J.-C. Tardif, A. Reid, M. M. Moloney, Expression and recovery of biologically active recombinant Apolipoprotein AI_{Milano} from transgenic safflower (*Carthamus tinctorius*) seeds. *Plant Biotechnol. J.* **9**, 250–263 (2011).
31. B. L. Sanchez-Gaytan, F. Fay, M. E. Lobatto, J. Tang, M. Ouimet, Y. T. Kim, S. E. M. van der Staay, S. M. van Rijs, B. Priem, L. Zhang, E. A. Fisher, K. J. Moore, R. Langer, Z. A. Fayad, W. J. M. Mulder, HDL-mimetic PLGA nanoparticle to target atherosclerosis plaque macrophages. *Bioconjug. Chem.* **26**, 443–451 (2015).
32. E. M. Degoma, D. J. Rader, Novel HDL-directed pharmacotherapeutic strategies. *Nat. Rev. Cardiol.* **8**, 266–277 (2011).
33. A. B. Nair, S. Jacob, A simple practice guide for dose conversion between animals and human. *J. Basic Clin. Pharm.* **7**, 27–31 (2016).
34. R. J. Corry, H. J. Winn, P. S. Russell, Primarily vascularized allografts of hearts in mice. The role of H-2D, H-2K, and non-H-2 antigens in rejection. *Transplantation* **16**, 343–350 (1973).
35. B.-S. Koo, D.-H. Lee, P. Kang, K.-J. Jeong, S. Lee, K. Kim, Y. Lee, J.-W. Huh, Y.-H. Kim, S.-J. Park, Y. B. Jin, S.-U. Kim, J.-S. Kim, Y. Son, S.-R. Lee, Reference values of hematological and biochemical parameters in young-adult cynomolgus monkey (*Macaca fascicularis*) and rhesus monkey (*Macaca mulatta*) anesthetized with ketamine hydrochloride. *Lab. Anim. Res.* **35**, 7 (2019).

Acknowledgments: We thank the Icahn School of Medicine at Mount Sinai, specifically the flow cytometry core, CCMS, and BioMedical Engineering and Imaging Institute's preclinical imaging core. **Funding:** This work was supported by NIH grants R01 CA220234, R01 HL144072, P01 HL131478, and NWO/ZonMW Vici 91818622 (to W.J.M.M.); R01 HL143814 and P01HL131478 (to Z.A.F.); R01 AI139623 (to J.O.); and P30 CA008748 (to T.R.). M.M.T.v.L. was supported by the American Heart Association (grant 19PRE34380423). M.G.N. was supported by a Spinoza grant from the Netherlands Organization for Scientific Research and an ERC Advanced Grant (no. 833247); L.A.B.J. was supported by a Competitiveness Operational Programme grant of the Romanian Ministry of European Funds (P_37_762, MySMIS 103587). **Author contributions:** A.B., M.E.B., E.D.K., G.P., R.R.M.J., and A.J.P.T. designed, formulated, (radio)labeled, and analyzed nanobiologics. M.M.T.v.L., A.E.M., E.M.v.L. V.P.M., and A.V.D.V. designed, performed, and analyzed in vitro experiments. M.M.T.v.L., Y.C.T., A.V.D.V., S.A.N., and J.M. performed and analyzed biodistribution, pharmacokinetics, PET imaging, and toxicity studies. M.M.T.v.L., Y.C.T., and F.O. performed transplantation studies. C.C., G.S., and P.M.R. developed and validated PET/MRI protocols. T.R., H.F., J.C.M., E.K., R.v.d.M., L.A.B.J., Z.A.F., M.G.N., J.O., and C.P.-M. provided methodology and resources, and assisted in interpreting the data. A.J.P.T. and W.J.M.M. supervised the study. A.J.P.T., W.J.M.M., and M.M.T.v.L. wrote the manuscript and produced the figures. All authors approved the final draft. **Competing interests:** W.J.M.M., L.A.B.J., J.O., M.G.N., and Z.A.F. are scientific founders of Trained Therapeutix Discovery. W.J.M.M., L.A.B.J., J.O., M.G.N., Z.A.F., C.P.-M., and A.J.P.T. are authors on the patent PCT/US2019/100044, "Inhibiting trained immunity with therapeutic nanobiologic composition," issued by the U.S. patent office, active since 23 May 2019. The authors declare no other competing interests. **Data and materials availability:** All data needed to evaluate the conclusions in the paper are present in the paper and/or the Supplementary Materials. The data that support the findings of this study are available from the corresponding authors upon request.

Submitted 15 September 2020
Accepted 21 January 2021
Published 5 March 2021
10.1126/sciadv.abe7853

Citation: M. M. T. van Leent, A. E. Meerwaldt, A. Berchouchi, Y. C. Toner, M. E. Burnett, E. D. Klein, A. V. D. Verschuur, S. A. Nauta, J. Munitz, G. Prévot, E. M. van Leeuwen, F. Ordikhani, V. P. Mourits, C. Calcagno, P. M. Robson, G. Soultanidis, T. Reiner, R. R. M. Joosten, H. Friedrich, J. C. Madsen, E. Kluza, R. van der Meel, L. A. B. Joosten, M. G. Netea, J. Ochando, Z. A. Fayad, C. Pérez-Medina, W. J. M. Mulder, A. J. P. Teunissen, A modular approach toward producing nanotherapeutics targeting the innate immune system. *Sci. Adv.* **7**, eabe7853 (2021).

ScienceAdvances

A modular approach toward producing nanotherapeutics targeting the innate immune system

Mandy M. T. van LeentAnu E. MeerwaldtAlexandre BerchouchiYohana C. TonerMarianne E. BurnettEmma D. KleinAnna Vera D. VerschuurSheqouia A. NautaJazz MunitzGeoffrey PrévotEsther M. van LeeuwenFarideh OrdikhaniVera P. MouritsClaudia CalcagnoPhilip M. RobsonGeorge SoultanidisThomas ReinerRick R. M. JoostenHeiner FriedrichJoren C. MadsenEwelina KluzaRoy van der MeelLeo A. B. JoostenMihai G. NeteaJordi OchandoZahi A. FayadCarlos Pérez-MedinaWillem J. M. MulderAbraham J. P. Teunissen

Sci. Adv., 7 (10), eabe7853. • DOI: 10.1126/sciadv.abe7853

Science Advances (ISSN 2375-2548) is published by the American Association for the Advancement of Science. 1200 New York Avenue NW, Washington, DC 20005. The title *Science Advances* is a registered trademark of AAAS.